About 3D Cavity Resonance

May 14, 2026

August 10, 2026 Revised

Takuya Yabu(takuya.yabu@live.jp)

Abstract

Research on automobile whistling and suction sounds has been conducted in the past. For cavity resonance, a type of whistling sound, the cavity resonance frequency has been determined using Rossiter's empirical formula. Therefore, we limited our study to the three-dimensional case and clarified the physical phenomena that arise by solving a set of partial differential equations that explain the phenomenon. As a result, we were able to determine the frequency at which resonance increases, taking into account three-dimensional space. Finally, we were able to confirm the conditions under which resonance increases through numerical calculations.

Nomenclature

L_x, L_y, L_z: Size of the hole in the x, y, and z directions.

ρ, c: Air density and air sound speed

ω: Angular frequency

f_x: Frequency obtained from Rossiter's formula

f_{xr}, f_y, f_z: Resonance frequencies in the x, y, and z directions

k: Wavenumber

t: Time

j: Imaginary unit

U, U_{vx}: Mainstream air velocity and vortex (vorticity) velocity

κ: Ratio of vortex (vorticity) velocity to mainstream air velocity

$\hat{G}_v(s)$: Fluid-driven gain

ϕ_v: Phase lag component of the fluid-driven gain

θ_{3D}: Phase lag component caused by the cavity space

M: Mach number

ζ: Vorticity

α: Efficiency of conversion from vorticity to sound pressure (dimension: L^2)

β: Efficiency of conversion from sound pressure to vorticity (dimension: $\mathrm{L}^2\mathrm{M}^{-1}\mathrm{T}^1$)

$\delta(x)$: Dirac delta function

$\delta'(x)$: Differential of Dirac delta function

$H(x)$: Heaviside step function

$u(x,y,z,t), v(x,y,z,t), w(x,y,z,t)$: Velocity in the x, y, and z directions

1. Introduction

In the past, research has been conducted on the whistling and suction sounds of automobiles (Calvo, Diaz, & San Roman, 2005) (Chien-Hsiung, Lung-Ming , Chang-Hsien , Yen-Loung , & Jik-Chang , 2009) (George, 1990) (Jagtiani, 1972) (Jung & Oh, 1995) (Münder & Carbon, 2022) (Oettle & Sims-Williams, 2017) (Qatu, Abdelhamid, Pang, & Sheng, 2009) (Wang, Chen, & Zhang, 2021) (Zhang, Meng, Li, & Zheng, 2022). Cavity resonance is a type of whistling sound. In cavity resonance, the cavity resonance frequency has traditionally been determined using Rossiter formula, an empirical formula. Therefore, for cavity resonance in the three-dimensional case, we will clarify the physical phenomena that arise by solving the set of partial differential equations that explain the phenomenon. Finally, we will examine the conditions under which resonance increases in numerical calculations.

These will be discussed below.

2. About 3D Cavity Resonance

2.1. Vorticity Movement Equation

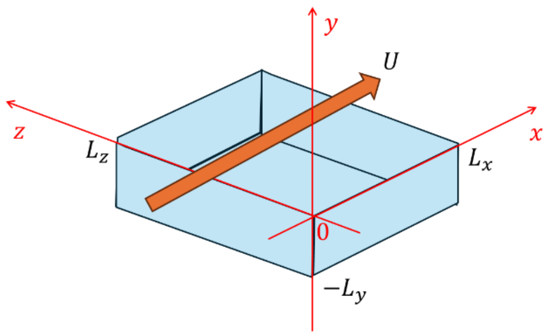

Fig. 1 3-Dimensional Box with Hole

Fig. 1 shows a box with a hole. Here, the conventional definitions of cavity resonance and cavity resonance frequency are given below.

Definition :

When air is flowing at velocity U and there is a hole, a vortex moves from the upstream end to the downstream end of the hole. This vortex collides with the downstream end, generating sound. This generated sound then moves from the downstream end to the upstream end. Sound is a change accompanied by particle velocity, and this particle velocity then collides with the upstream end, generating another vortex. This series of phenomena is defined as "cavity resonance." Furthermore, the reciprocal of the time from when a vortex moves and generates sound until another vortex is generated is defined as the "cavity resonance frequency."

Based on this definition, we derive the differential equation representing cavity resonance, limited to three dimension. First, the movement equation of vorticity $\zeta_z(x, y, z, t)$ is expressed by the following equation. However, the viscosity term is ignored. Furthermore, $\zeta_z(x, y, z, t)$ is the vorticity around the z-axis.

$$\frac{\partial \zeta_z}{\partial t} + U_{vx} \frac{\partial \zeta_z}{\partial x} = 0 \tag{1}$$

2.2. Powell's Equation

Next, we will find the relationship between sound pressure and vorticity.

Powell's equation is the relationship between sound pressure and vorticity. Expressed in three dimension, Powell's equation is given by the following:

$$\frac{1}{c^2}\frac{\partial^2 p}{\partial t^2} - \left(\frac{\partial^2 p}{\partial x^2} + \frac{\partial^2 p}{\partial y^2} + \frac{\partial^2 p}{\partial z^2}\right)$$
$$= \alpha\rho \sin\left(\frac{\pi z}{L_z}\right)[\zeta_z(L_x, 0, z, t)u(L_x, 0, z, t)\delta'(x - L_x)\delta(y)$$
$$-\zeta_z(L_x, 0, z, t)v(L_x, 0, z, t)\delta(x - L_x)\delta'(y)] \tag{2}$$

2.3. Initial Conditions

The initial condition for the velocity in the x-direction is given below:

$$u(x, y \geq 0, 0) = U \tag{3}$$

The initial condition for the velocity in the y-direction is given below:

$$v(x, y, 0) = 0 \tag{4}$$ z

The initial condition for the velocity in the z-direction is given below:

$$w(x, y, z, 0) = 0 \tag{5}$$

The initial condition for the sound pressure is given below:

$$p(x, y, 0) = 0 \tag{6}$$

The initial condition for the time derivative of the sound pressure is given below:

$$\left.\frac{\partial p}{\partial t}\right|_{t=0} = 0 \tag{7}$$

2.4. Boundary Conditions

We need to find the boundary conditions under which the velocity of the returned particles changes to vorticity. These are given by the following equation:

$$\zeta(0,0,0 \le z \le L_z, t) = -\beta_x \left.\frac{\partial p}{\partial x}\right|_{(x=0,y=0,t=t)} \tag{8}$$

Furthermore, assuming that sound pressure is completely reflected at the bottom of the box and becomes zero at the open end, the following conditions hold true.

$$\left.\frac{\partial p}{\partial x}\right|_{y=-L_y} = 0 \tag{9}$$

Furthermore, assuming that the sound pressure is completely reflected by the front and back walls, the following conditions hold true.

$$\left.\frac{\partial p}{\partial x}\right|_{x=0,-L_y\le y\le 0} = 0 \tag{10}$$

$$\left.\frac{\partial p}{\partial x}\right|_{x=L_H,-L_y\le y\le 0} = 0 \tag{11}$$

Furthermore, assuming that the sound pressure is completely reflected by the left and right walls, the following conditions hold true.

$$\left.\frac{\partial p}{\partial z}\right|_{z=0,-L_y\le y\le 0} = 0 \tag{12}$$

$$\left.\frac{\partial p}{\partial z}\right|_{z=L_z,-L_y\le y\le 0} = 0 \tag{13}$$

3. Resonance Frequency of a Three-Dimensional Cavity Resonance

3.1. Solution to the Vorticity Transfer Equation

We derive the resonance frequency of a two-dimensional cavity resonance. First, we solve equation (1). The solution when the boundary condition is $\zeta(0,t)$ is given by the following equation:

$$\zeta_z(x,y,z,t) = \zeta_z\left(0,0,z,t-\frac{x}{U_{vx}}\right) \tag{14}$$

3.2. Sound Pressure Equation Using Green's Function Derived from Powell's Equation

Next, we solve Powell's equation (2). This can be obtained using the Green's function in the following form. First, the Green's function is given by the following equation.

$$G(x,y,z,t|x',y',z',\tau)=\frac{c}{4\pi r}\delta(c(t-\tau)-r) \tag{15}$$

Here, the following equation holds true.

$$r=\sqrt{(x-x')^2+(y-y')^2+(z-z')^2} \tag{16}$$

From equations (2) and (15), the following equation is obtained.

$$p(x,y,z,t)=\sum_{n=-\infty}^{\infty}\sum_{k=-\infty}^{\infty}\left[-\int_0^1 P_{n,m=0,k}(t)d\tilde{z}+\int_0^1 P_{n,m=1,k}(t)d\tilde{z}\right] \tag{17}$$

Here, the following equation holds true.

$$P_{n,m,k}(t)=\frac{\alpha\rho L_x L_y}{4\pi r_{n,m,k}}\left[\frac{1}{c}\frac{\partial}{\partial t}\{\Phi_{n,m,k}(\tau_{n,m,k})\}+\frac{1}{r_{n,m,k}}\{\Phi_{n,m,k}(\tau_{n,m,k})\}\right] \tag{18}$$

$$\tau_{n,m,k}=t-\frac{r_{n,m,k}}{c} \tag{19}$$

$$\Phi_{n,m,k}(\tau)=\sin(\pi\tilde{z})\,\zeta_z(L_x,0,\tilde{z}L_z,\tau_{n,m,k})$$
$$\times\left\{\frac{u(L_x,0,\tilde{z}L_z,\tau_{n,m,k})\cdot(x-(2n+1)L_x)-(-1)^{n+k}\cdot v(L_H,0,\tilde{z}L_z,\tau_{n,m,k})\cdot(y-Y_m)}{c^2(t-\tau_{n,m,k})^2-r_{n,m,k}^2}\right\} \tag{20}$$

$$r_{n,m,k}=\sqrt{(x-(2n+1)L_x)^2+(y-Y_m)^2+(\tilde{z}L_z-2kL_z)^2} \tag{21}$$

$$Y_0=0,Y_1=-2L_y \tag{22}$$

3.3. Stability Condition and Frequency in the Mainstream Air Velocity Direction and Cavity Resonance Frequency

We consider the stability condition for the solution obtained from Equation (17). Applying the Laplace transform to both sides yields the following equation, where we set $u(L_H,0,\tilde{z}L_z,s)=U$. Furthermore, to analyze the stability condition, we assume $\zeta_z(L_H,0,\tilde{z}L_z,s)=\zeta_{z0}e^{st}$ and $v(L_H,0,\tilde{z}L_z,s)=v_0e^{st}$. Here, consistent with linear theory, terms involving e^{2st} are neglected as infinitesimal quantities.

$$p(x,y,z,s)=\frac{\alpha\rho L_x L_y U\zeta_{z0}x}{4\pi}e^{st}\sum_{n=-\infty}^{\infty}\sum_{k=-\infty}^{\infty}[-\int_0^1\sin(\pi\tilde{z})\cdot e^{-\frac{r_{n,0,k}}{c}s}\left(\frac{s}{cr_{n,0,k}}+\frac{1}{r_{n,0,k}^2}\right)d\tilde{z}$$
$$+\int_0^1\sin(\pi\tilde{z})\cdot e^{-\frac{r_{n,1,k}}{c}s}\left(\frac{s}{cr_{n,1,k}}+\frac{1}{r_{n,1,k}^2}\right)d\tilde{z}] \tag{23}$$

Considering that self-excited oscillations arise when a vortex generated at the upstream edge of the cavity—relative to the mainstream flow—strikes the downstream edge to produce sound, and that sound then travels back from the downstream edge to the upstream edge, the following equation is obtained. Here, we assume $p(x,y,z,s)=p_0e^{st}$.

$$p_0e^{st}=-\frac{\alpha\rho L_x L_y U\zeta_{z0}x}{4\pi}e^{st}e^{-s\left(\frac{L_x}{U_{vx}}+\frac{L_x}{c}\right)}$$

$$\times \sum_{n=-\infty}^{\infty} \sum_{k=-\infty}^{\infty} [\int_0^1 \sin(\pi\tilde{z}) \cdot e^{-\frac{r_{n,0,k}}{c}s} \left(\frac{s}{cr_{n,0,k}} + \frac{1}{r_{n,0,k}^2}\right) d\tilde{z}$$

$$- \int_0^1 \sin(\pi\tilde{z}) \cdot e^{-\frac{r_{n,1,k}}{c}s} \left(\frac{s}{cr_{n,1,k}} + \frac{1}{r_{n,1,k}^2}\right) d\tilde{z}] \tag{24}$$

Therefore, letting $\hat{G}_v(s)$ represent the fluid-driven gain, the characteristic equation is given by the following expression:

$$1 - \hat{G}_v(s)\{-\frac{\alpha\rho L_x L_y U \zeta_{z0} x}{4\pi} e^{st} e^{-s\left(\frac{L_x}{U_{vx}} + \frac{L_z}{c}\right)}$$

$$\times \sum_{n=-\infty}^{\infty} \sum_{k=-\infty}^{\infty} [\int_0^1 \sin(\pi\tilde{z}) \cdot e^{-\frac{r_{n,0,k}}{c}s} \left(\frac{s}{cr_{n,0,k}} + \frac{1}{r_{n,0,k}^2}\right) d\tilde{z}$$

$$- \int_0^1 \sin(\pi\tilde{z}) \cdot e^{-\frac{r_{n,1,k}}{c}s} \left(\frac{s}{cr_{n,1,k}} + \frac{1}{r_{n,1,k}^2}\right) d\tilde{z}]\} = 0 \tag{25}$$

Consider the frequency f_x in the mainstream air direction. In this case, the following equation holds based on Equation (25). Here, ϕ_v represents the phase lag component of the fluid-driven gain, and θ_{3D} represents the phase lag component caused by the cavity space.

$$-\phi_v - \theta_{3D} - \omega\left(\frac{L_x}{U_{vx}} + \frac{L_x}{c}\right) = -2\pi n$$

$$2\pi\left(n - \frac{\phi_v + \theta_{3D}}{2\pi}\right) = 2\pi f_x\left(\frac{L_x}{U_{vx}} + \frac{L_x}{c}\right)$$

$$f_x = \frac{\left(n_x - \frac{\phi_v + \theta_{3D}}{2\pi}\right)}{\frac{L_x}{U_{vx}} + \frac{L_x}{c}} \tag{26}$$

Finally, by setting $U_{vx} = \kappa U$, the following equation is obtained. Conventionally, a value of 0.25 or close to it has been used for the phase lag in Rossiter's formula. Based on stability conditions, however, it was possible to derive from Equation (25) that $\frac{\phi_v+\theta_{3D}}{2\pi}$ should be used as the phase lag in Rossiter's formula.

$$f_x = \frac{U}{L_x} \frac{\left(n_x - \frac{\phi_v + \theta_{3D}}{2\pi}\right)}{\left(\frac{1}{\kappa} + \frac{U}{c}\right)} \tag{27}$$

Next, applying Poisson's summation formula to Equation (25) yields the following equation.

$$1 - \hat{G}_v(s)\{-\frac{\alpha\rho L_x L_y U \zeta_{z0} x}{4\pi} e^{st} e^{-s\left(\frac{L_x}{U_{vx}} + \frac{L_x}{c}\right)}$$

$$\times\left(1-e^{-s\left(\frac{2L_y}{c}\right)}\right)\sum_{n=-\infty}^{\infty}\sum_{k=-\infty}^{\infty}[\frac{1}{s^2+\left(\frac{n\pi c}{L_x}\right)^2}\cdot\frac{1}{s^2+\left(\frac{k\pi c}{L_z}\right)^2}\{\frac{s}{c}\cdot\cos\left(\frac{n\pi|y|}{L_x}\right)\sin\left(\frac{k\pi z}{L_z}\right)$$

$$+\frac{s^2\pi}{L_z\left(s^2+\left(\frac{k\pi c}{L_z}\right)^2\right)}\cdot\sin\left(\frac{n\pi|y|}{L_x}\right)\cos\left(\frac{k\pi z}{L_z}\right)\}]=0 \tag{28}$$

Substituting $s = j\omega$ into this equation to analyze the stability conditions reveals that the expression diverges to infinity when:

$$\omega = \frac{n\pi c}{L_x} \tag{29}$$

Here, substituting $\omega = 2\pi f_{xr}$ and $n = n_{xr}$ yields the following equation:

$$f_{xr} = \frac{n_{xr}c}{2L_x} \tag{30}$$

At this frequency, cavity resonance—a form of self-excited oscillation—occurs. This frequency corresponds to the resonance frequency in the x-direction.

Similarly, divergence occurs in the following case:

$$\omega = \frac{k\pi c}{L_z} \tag{31}$$

Substituting $\omega = 2\pi f_z$ and $k = n_z$ here yields the following equation:

$$f_z = \frac{n_z c}{2L_z} \tag{32}$$

At this frequency, cavity resonance—a form of self-excited oscillation—occurs. This corresponds to the resonance frequency in the z-direction.

Finally, consider only the term $1-e^{-s\left(\frac{2L_y}{c}\right)}$ from Equation (28). Focusing solely on this part yields the following equation (where $s = j\omega$ is substituted):

$$1-\Lambda(s)\left(1-e^{-s\left(\frac{2L_y}{c}\right)}\right)=0$$

$$1-e^{-s\left(\frac{2L_y}{c}\right)}=\frac{1}{\Lambda(s)}$$

$$e^{-s\left(\frac{2L_y}{c}\right)}=1-\frac{1}{\Lambda(s)}=R(s)$$

$$e^{-j\omega\left(\frac{2L_y}{c}\right)}=R(j\omega) \tag{33}$$

In this case, self-excited oscillation occurs when $R(j\omega) = -1$. Therefore, the following equation holds:

$$\omega\left(\frac{2L_y}{c}\right) = (2l-1)\pi \tag{34}$$

Substituting $\omega = 2\pi f_y$ and $l = n_y$ here yields the following equation:

$$f_y = \frac{(2n_y - 1)c}{4L_y} \tag{35}$$

At this frequency, cavity resonance—a form of self-excited oscillation—occurs. This corresponds to the resonance frequency in the y-direction.

Unlike the resonance frequencies of a standard enclosed space, the frequency f_x associated with the main flow direction arises first. When this frequency matches the resonance frequency along any of the axes, a lock-in phenomenon occurs, resulting in loud sound generation. Of course, when degeneracy occurs—where the resonant frequencies along each axis are equal—the lock-in phenomenon generates an even louder sound.

3.4. Sound Pressure at a Position Outside the Sound Source ($x \geq L_x$)

We will now discuss the sound pressure at a position outside the sound source ($x \geq L_x$). As before, it can be calculated using the following equation.

$$p(x,y,z,t) = -\int_0^1 \frac{\alpha\rho}{4\pi r_{3D}(\tilde{z})}\{\frac{1}{c}\frac{\partial}{\partial t}\Phi_{3D}(x,y,\tilde{z},\tau_{3D})$$

$$+\frac{1}{r_{3D}(z')}[\Phi_{3D}(x,y,\tilde{z},\tau_{3D})]\}d\tilde{z} \tag{36}$$

Here, the following equation holds.

$$r_{3D}(\tilde{z}) = \sqrt{(x-L_x)^2 + y^2 + (z-\tilde{z}L_z)^2} \tag{37}$$

$$\tau_{3D} = t - \frac{r_{3D}(\tilde{z})}{c} \tag{38}$$

$$\Phi_{3D}(x,y,\tilde{z},\tau_{3D}) =$$

$$(u(L_x,0,\tilde{z}L_z,t)\cdot(x-L_x) - v(L_x,0,\tilde{z}L_z,\tau_{3D})\cdot y)\sin(\pi\tilde{z})\,\zeta_z(L_x,0,\tilde{z}L_z,\tau_{3D}) \tag{39}$$

4. Numerical Calculations

The results were confirmed by numerical calculation. The values used are shown in Table 1 below.

Furthermore, for $\frac{\partial p}{\partial x}$ and $v(L_x,0,z,t)$, it was assumed that vortices were continuously generated at the upstream end at a Rossiter formula primary frequency of 9.6 (Hz), and that this vortex mass was continuously excited at the downstream end as $v(L_x,0,z,t)$ at the same Rossiter formula primary frequency of 9.6 (Hz). Therefore, the following equation is continuously used during the numerical calculation. Here, $f_{x,1}$ is the Rossiter formula primary frequency of 9.6 (Hz).

$$\frac{\partial p}{\partial x} = \sin(2\pi f_{x,1} t) \tag{40}$$

$$v(L_x, 0, z, t) = \frac{1}{2} \sin\left(\frac{\pi z}{L_z}\right) \sin(2\pi f_{x,1} t) \tag{41}$$

Table 1 Parameter and Value

Parameter	Value
ρ	1.225(kg/m^3)
c	340.0(m/s)
U	34.0(m/s)
κ	0.6
α	1(m^2)
β_x	0.01(m^{2}s/kg)
$\phi_v + \theta_{3D}$	$\frac{\pi}{2}$
L_x	1.5(m)
L_y	0.7(m)
L_z	1.3(m)

The numerical calculation results are shown in Fig. 2. The observation position was $(x, y, z) = (0.01, 0.01, 0.01)$ near the origin. The top graph shows the time-series waveform of sound pressure, and the bottom graph shows the frequency characteristics of sound pressure.

The time-series waveform of the sound pressure in Fig. 2 shows a peak occurring almost exclusively at the fundamental frequency f_x. This indicates that the frequency in the dominant direction is excited and that the lock-in phenomenon is not occurring.

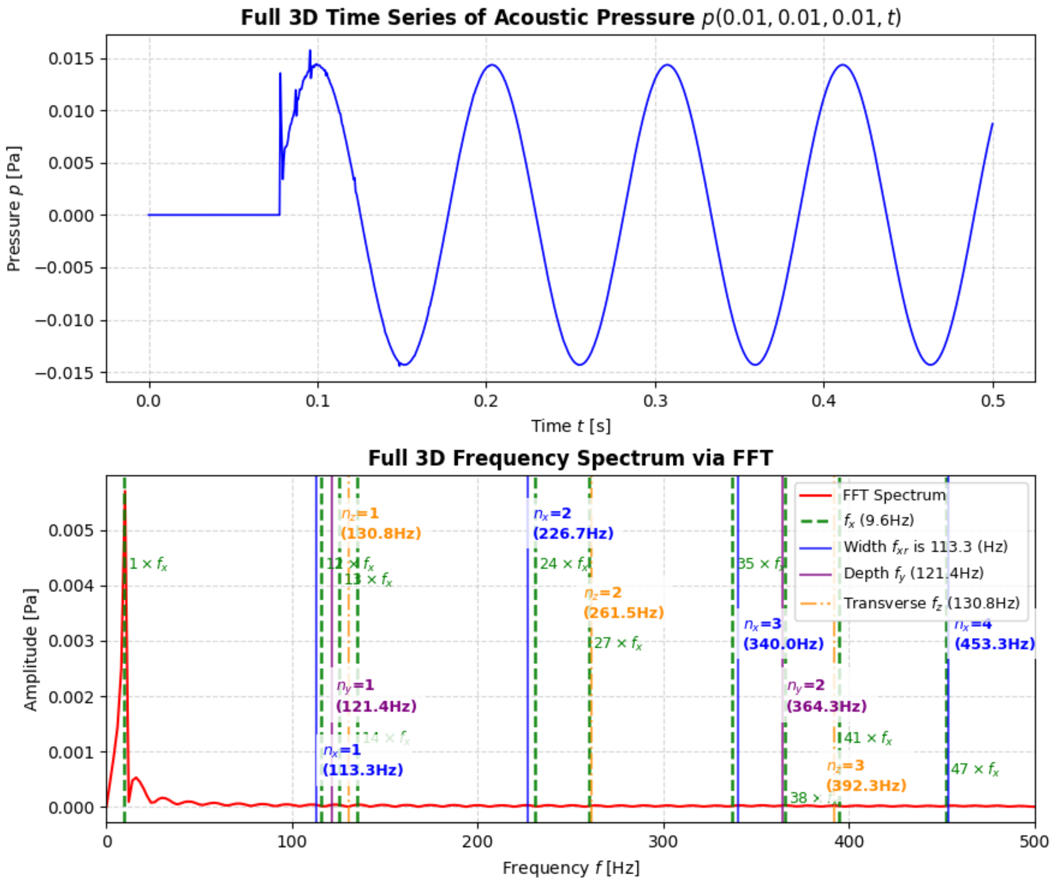

Fig. 2 Numerical Calculation Results

Next, we calculate the sound pressure for $x \geq L_x$. The results are shown in Fig. 3. The observation position was $(x, y, z) = (2.0, 0.5, 0.6)$. The top graph shows the time-series waveform of the sound pressure, and the bottom graph shows the frequency response of the sound pressure.

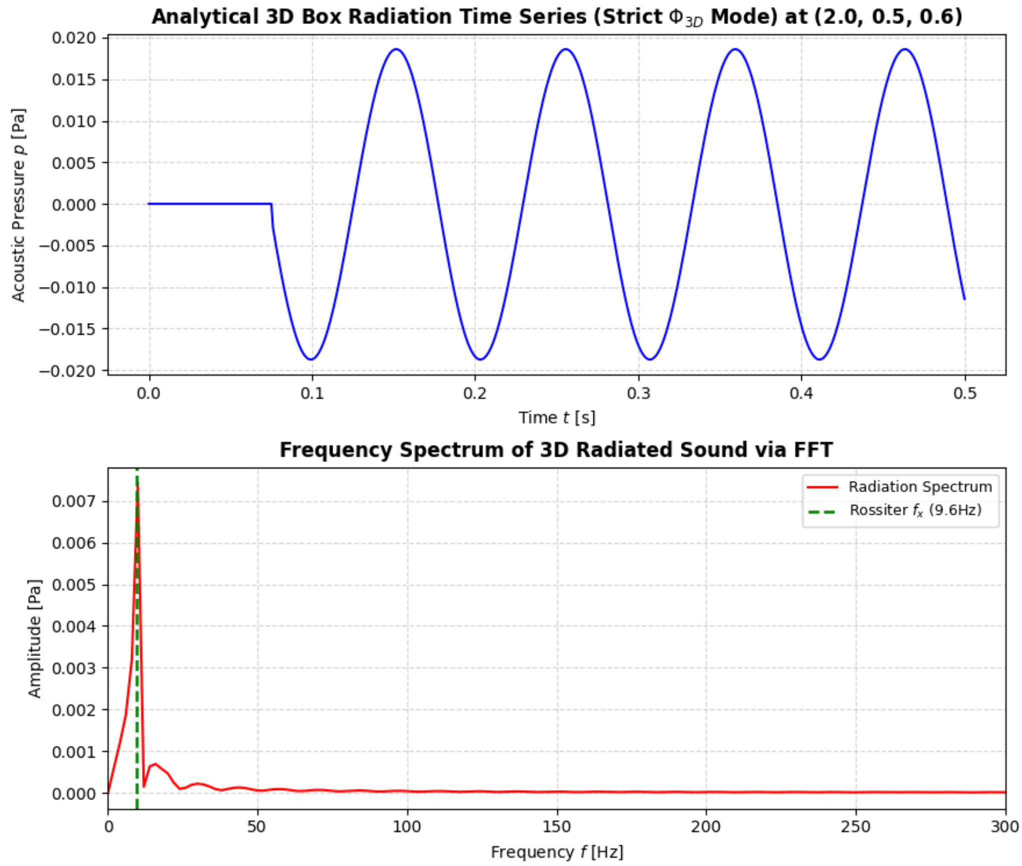

Fig. 3 Numerical Calculation Result ($(x, y, z) = (2.0, 0.5, 0.6)$)

Looking at the top graph in Fig. 3, we can see that time is required for the sound to reach the source. Also, from the frequency response below, a peak at 9.6 (Hz) appears, corresponding to the first frequency of Rossiter formula f_x. That is, for $x \geq L_x$, the sound has a frequency component at the first frequency of Rossiter formula f_x, which is the frequency of forced oscillation.

Next, Fig. 4 presents the numerical calculation results for $U = 1132.3$ (m/s), with the observation point set near the origin at $(x, y, z) = (0.01, 0.01, 0.01)$. The time-series waveforms and frequency characteristics reveal that the fundamental frequency of f_x and the fundamental resonance frequency of f_{xr} coincide and that the sound generated is louder than that shown in Fig. 2; in other words, a lock-in phenomenon is occurring. No significant peaks are observed for other orders of f_{xr}, or for f_y and f_z. Furthermore, sound pressures on the order of 10^8 (Pa) are not generated. This suggests a balance between the energy of the sound generated by the source terms (distributed along $x = L_x, y = 0, 0 \leq z \leq L_z$) and the energy of the sound dissipating outward into the external space as spherical waves; the generated sound energy does not become dominant. Although a sound pressure of 4.5 (Pa) appears at the moment sound generation begins, this is attributed to the fact that energy has not yet dissipated from the source terms into the external space. Subsequently, the sound amplitude settles to approximately 2 (Pa) due to mutual cancellation effects and the dissipation of sound energy into the external space.

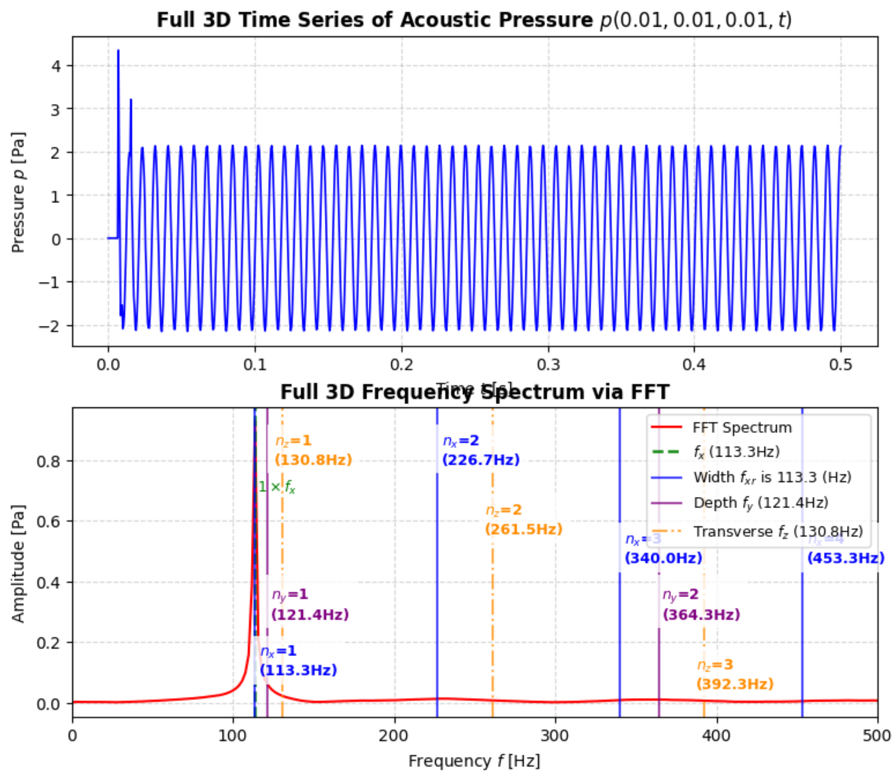

Fig. 4 Numerical Calculation Result (U = 1132.3(m/s))

Next, Fig. 5 shows the numerical calculation results for 1250.9 (m/s), with the observation point set at $(x, y, z) = (0.01, 0.01, 0.01)$ near the origin. The first-order resonant frequency of f_x lies at 117.0 Hz—a frequency situated between the first-order resonant frequencies of f_{xr} and f_y—and its amplitude is approximately 0.5 (Pa) greater than that of f_x shown in Fig. 4. Consequently, no significant peaks appear for f_{xr}, f_y, or f_z. The graphs of the time-series waveforms and frequency characteristics reveal that a phenomenon similar to the one discussed in Fig. 4 is occurring.

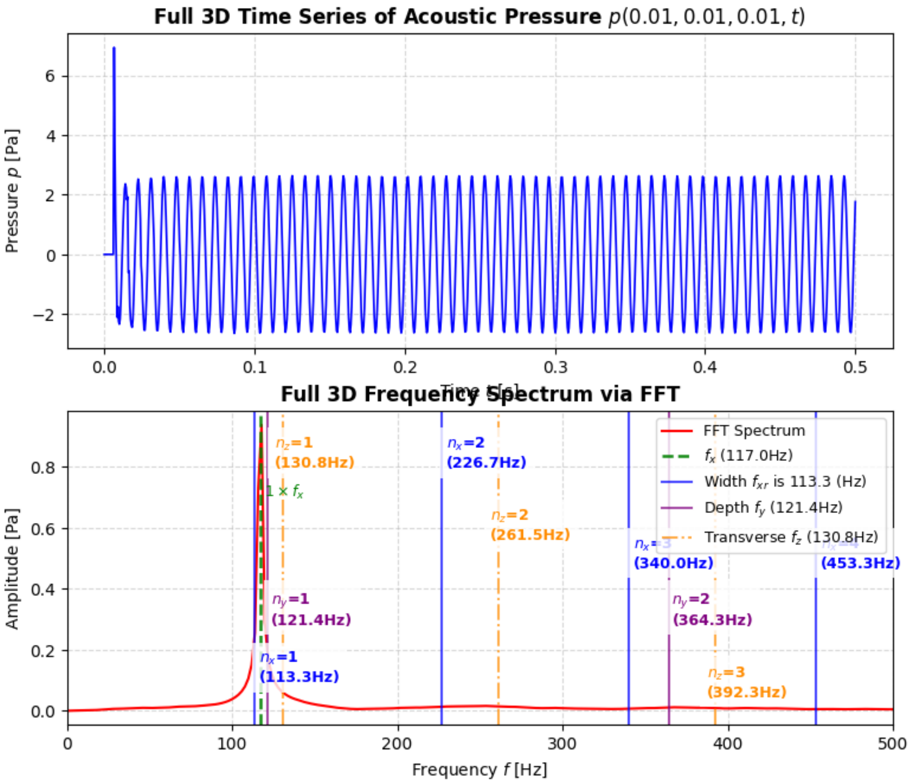

Fig. 5 Numerical Calculation Result (U = 1250.9(m/s))

Next, Fig. 6 shows the numerical calculation results for $U = 1415.5$ (m/s), with the observation point set at $(x, y, z) = (0.01, 0.01, 0.01)$ near the origin. A peak appears where the fundamental frequency of f_x and the fundamental resonant frequency of f_y coincide, and the amplitude is approximately 1 (Pa) greater than that of f_x in Fig. 4. As before, no significant peaks appear in other orders of f_y, or in f_{xr} or f_z. The graphs of the time-series waveforms and frequency characteristics reveal that a phenomenon similar to the one discussed in Fig. 4 is occurring.

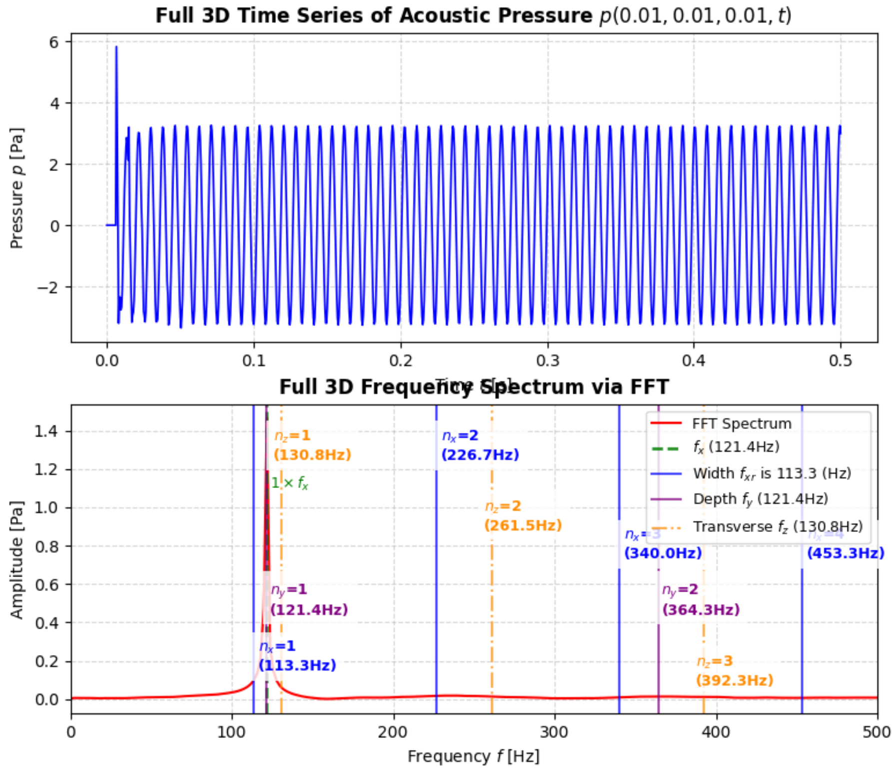

Fig. 6 Numerical Calculation Result (U = 1415.5(m/s))

Finally, Fig. 7 shows the numerical calculation result for $U = 1890.8$ (m/s), with the observation point set at $(x, y, z) = (0.01, 0.01, 0.01)$, near the origin. A peak appears where the fundamental frequency of f_x coincides with the fundamental resonance frequency of f_z, and the amplitude is approximately 3 Pa greater than that of f_x in Fig. 4. As before, no significant peaks are observed in other orders of f_z, or in f_{xr} or f_y. The graphs of the time-series waveforms and frequency characteristics reveal that a phenomenon similar to the one discussed in Fig. 4 is occurring.

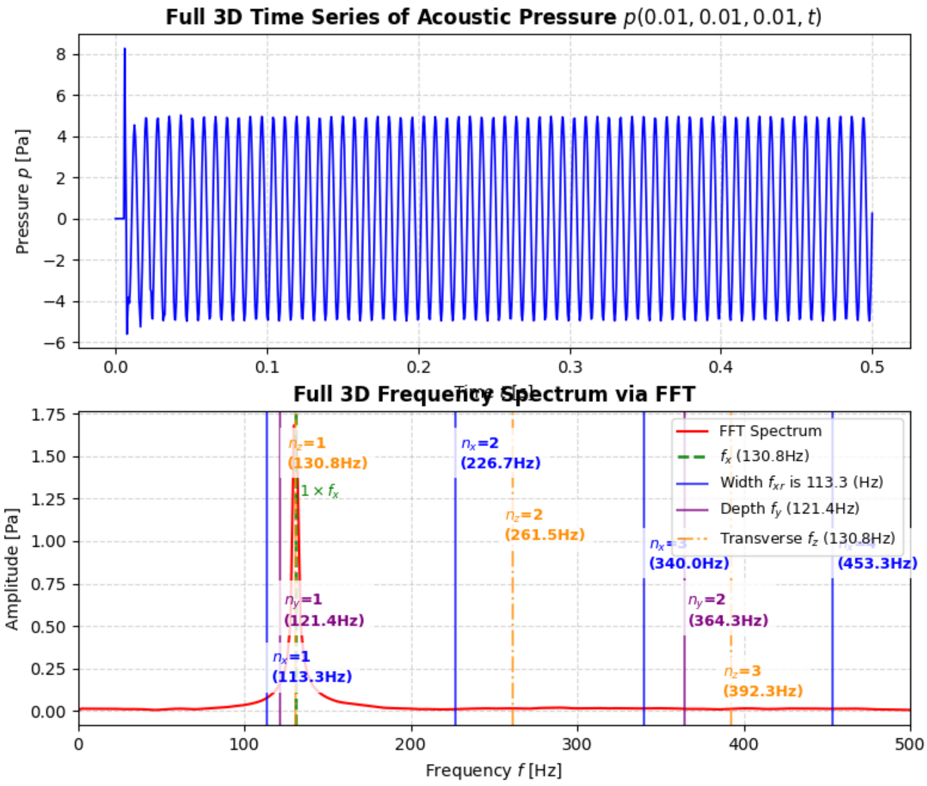

Fig. 7 Numerical Calculation Result ($U = 1890.8$(m/s))

5. Derivation of α and β_x

Here, we derive α and β_x.

Applying the quasi-static assumption to Equation (2) yields the following equation:

$$-\left(\frac{\partial^2 p}{\partial x^2}+\frac{\partial^2 p}{\partial y^2}+\frac{\partial^2 p}{\partial z^2}\right)$$

$$= \alpha\rho\sin\left(\frac{\pi z}{L_z}\right)[\zeta_z(L_x,0,z,t)u(L_x,0,z,t)\delta'(x-L_x)\delta(y)$$

$$-\zeta_z(L_x,0,z,t)v(L_x,0,z,t)\delta(x-L_x)\delta'(y)] \tag{42}$$

Solving Equation (42) and substituting $x = 0, y = 0$ yields the following equation:

$$\left.\frac{\partial p}{\partial x}\right|_{x=0,y=0} = \frac{\alpha\rho}{4\pi}\int_0^{L_z}\sin\left(\frac{\pi z'}{L_z}\right)\zeta_z(L_x,0,z',t)u(L_x,0,z',t)\frac{z'^2-2L_x^2}{(L_x^2+z'^2)^{\frac{5}{2}}}dz' \tag{43}$$

Here, given that $u(x, y \geq 0, 0) = U$, the following equation is obtained.

$$\left.\frac{\partial p}{\partial x}\right|_{x=0,y=0} = \frac{\alpha\rho U}{4\pi}\int_0^{L_z} \sin\left(\frac{\pi z'}{L_z}\right)\zeta_z(L_x,0,z',t)\frac{z'^2 - 2L_x^2}{\left(L_x^2 + z'^2\right)^{\frac{5}{2}}}dz' \tag{44}$$

Therefore, based on Equations (44) and (8), we perform a mathematical transformation assuming that the vorticity does not change as it flows from the upstream end to the downstream end:

$$\left.\frac{\partial p}{\partial x}\right|_{x=0,y=0} = \frac{\alpha\rho U}{4\pi}\int_0^{L_z} \sin\left(\frac{\pi z'}{L_z}\right)\zeta_z(0,0,z',t)\frac{z'^2 - 2L_x^2}{\left(L_x^2 + z'^2\right)^{\frac{5}{2}}}dz'$$

$$\left.\frac{\partial p}{\partial x}\right|_{x=0,y=0} = \frac{\alpha\rho U}{4\pi}\int_0^{L_z} \sin\left(\frac{\pi z'}{L_z}\right)\left(-\beta_x \left.\frac{\partial p}{\partial x}\right|_{x=0,y=0}\right)\frac{z'^2 - 2L_x^2}{\left(L_x^2 + z'^2\right)^{\frac{5}{2}}}dz'$$

Here, since $\alpha\beta_x \left.\frac{\partial p}{\partial x}\right|_{x=0,y=0}$ is a value that depends only on time, it can be moved outside the integral. Consequently, the following equation is obtained:

$$\left.\frac{\partial p}{\partial x}\right|_{x=0,y=0} = -\alpha\beta_x \left.\frac{\partial p}{\partial x}\right|_{x=0,y=0} \times \frac{\rho U}{4\pi}\int_0^{L_z} \sin\left(\frac{\pi z'}{L_z}\right)\frac{z'^2 - 2L_x^2}{\left(L_x^2 + z'^2\right)^{\frac{5}{2}}}dz'$$

$$\therefore \beta_x = -\frac{4\pi}{\alpha\rho U\mathcal{J}} \tag{45}$$

Here, $\mathcal{J}$ is given by the following equation:

$$\mathcal{J} = \int_0^{L_z} \sin\left(\frac{\pi z'}{L_z}\right)\frac{z'^2 - 2L_x^2}{\left(L_x^2 + z'^2\right)^{\frac{5}{2}}}dz' \tag{46}$$

Now, regarding Equation (2), the equation obtained by integrating both sides with respect to y and z is as follows, where $\bar{p} = \int_0^{L_z}\int_{-L_y}^{\infty} p dy\, dz$. This derivation utilizes the fact that the sound pressure gradient is zero at $y = -L_y, z = 0$, and $= L_z$ due to perfect sound reflection, and also zero at $y = \infty$ due to sound diffusion.

$$\frac{1}{c^2}\frac{\partial^2 \bar{p}}{\partial t^2} - \frac{\partial^2 \bar{p}}{\partial x^2} - \int_0^{L_z}\left(\left.\frac{\partial p}{\partial y}\right|_{y=\infty} - \left.\frac{\partial p}{\partial y}\right|_{y=-L_y}\right)dz - \int_{-L_y}^{\infty}\left(\left.\frac{\partial p}{\partial z}\right|_{z=L_z} - \left.\frac{\partial p}{\partial z}\right|_{z=0}\right)dy$$

$$= \alpha\rho\left(\frac{2L_z}{\pi}\right)\zeta_z(L_x,t)u(L_x,t)\delta'(x - L_H)$$

$$\therefore \frac{1}{c^2}\frac{\partial^2 \bar{p}}{\partial t^2} - \frac{\partial^2 \bar{p}}{\partial x^2} = \alpha\rho U\left(\frac{2L_z}{\pi}\right)\zeta_z(L_x,t)\delta'(x - L_H) \tag{47}$$

By considering the case analogous to one-dimensional cavity resonance (Yabu, 2026) and applying Howe's vortex sound theory, α is determined as follows. Here, $\mathcal{G}_{space}$ is a positive geometric coefficient derived from the sharpness of the edge. The phase lag occurring during the conversion from vortex to sound is assumed to be zero. Additionally, α is negative to ensure consistency in the polarity of the conversion from vorticity to sound pressure as defined in Equation (45).

$$\alpha = -\mathcal{G}_{space} \cdot M \cdot \left(\frac{2L_z}{\pi}\right) \tag{48}$$

Therefore, β_x is given by the following equation:

$$\beta_x = \frac{2\pi^2}{L_z \cdot \mathcal{G}_{space} \cdot M \cdot \rho U \mathcal{J}} \tag{49}$$

Now, using Equation (47) to derive the characteristic equation—analogous to that for one-dimensional cavity resonance—we obtain the following result (Yabu, 2026). Note that since β_x has been reduced, $\beta = \frac{1}{\rho U}$. Furthermore, because the cavity edge is right-angled, $\mathcal{G}_{space} = \frac{2}{3}$

$$1 = \frac{\alpha\beta\rho U}{2c} \cdot s \cdot e^{s\left(-\frac{L_x}{U_{vx}} - \frac{L_x}{c}\right)}$$

$$\therefore 1 = \frac{2L_z M}{3\pi c} \cdot s \cdot e^{s\left(-\frac{L_x}{U_{vx}} - \frac{L_x}{c}\right)} \tag{50}$$

By deriving the Rossiter's formula (f_c) and the stability condition equation (G) in a manner similar to one-dimensional cavity resonance (Yabu, 2026), we obtain the following:

$$f_c = \frac{U}{L_x} \frac{n - \frac{1}{4}}{\left(\frac{1}{\kappa} + M\right)} \tag{51}$$

$$G = \frac{2L_z M\omega}{3\pi c} \tag{52}$$

Fig. 8 shows a graph where L_x is plotted on the horizontal axis and G on the vertical axis, with ω calculated using Equation (52) and setting $n = 1$ in Equation (51). This indicates that the system is unstable when L_x is less than 7.36(mm) and stable when it is greater. This value of L_x is determined by the following equation:

$$L_x = \frac{4}{3} L_z M \frac{(1 - 0.25)}{\left(\frac{c}{\kappa U} + 1\right)} \tag{53}$$

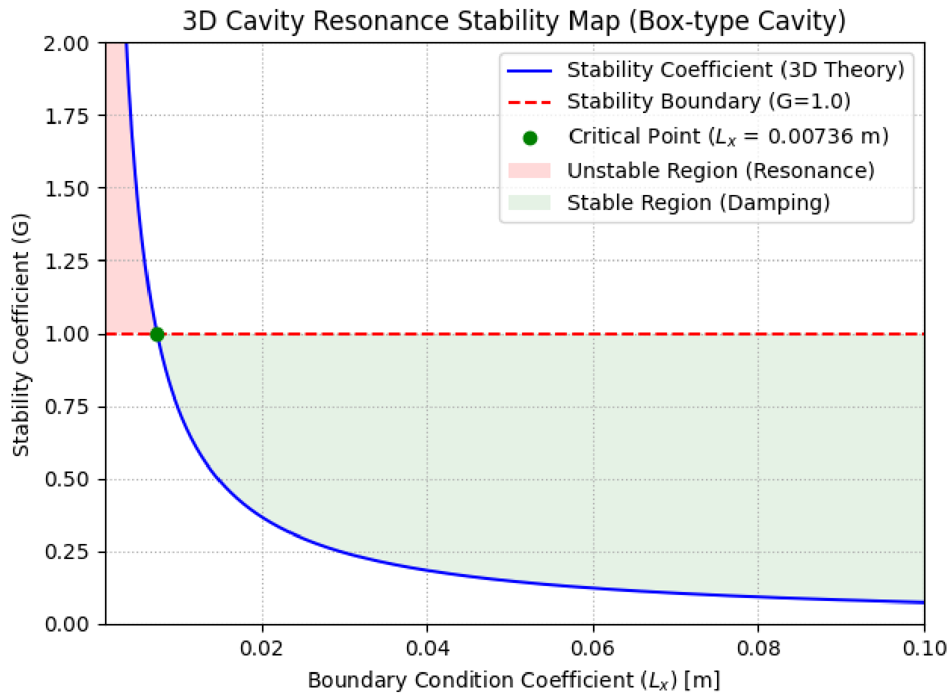

Fig. 8 Numerical Calculation Result (Stability Check)

Thus, α is determined by Equation (48), and β_x is determined by Equation (49).

6. Conclusion

Research on automobile whistling and suction sounds has been conducted in the past. For cavity resonance, a type of whistling sound, the cavity resonance frequency has been determined using Rossiter's empirical formula. Therefore, we limited our study to the three-dimensional case and clarified the physical phenomena that arise by solving a set of partial differential equations that explain the phenomenon. As a result, we were able to determine the frequency at which resonance increases, taking into account three-dimensional space. Finally, we were able to confirm the conditions under which resonance increases through numerical calculations.

References

Calvo, J. A., Diaz, V., & San Roman, J. L. (2005). *Controlling the turbocharger whistling noise in diesel engines.* International Journal of Vehicle Noise and Vibration, Vol. 2, No. 1. doi:https://doi.org/10.1504/IJVNV.2006.008524

Chien-Hsiung, T., Lung-Ming , F., Chang-Hsien , T., Yen-Loung , H., & Jik-Chang , L.

(2009). *Computational aero-acoustic analysis of a passenger car with a rear spoiler.* Applied Mathematical Modelling, Volume 33, Issue 9. doi:https://doi.org/10.1016/j.apm.2008.12.004

George, A. R. (1990). *Automobile Aerodynamic Noise.* SAE Transactions, Vol. 99, Section 6. Retrieved from http://www.jstor.org/stable/44553993

Jagtiani, H. (1972). *The Objective Method of Evaluating Aspiration Wind Noise.* SAE Technical Paper 720506. doi:https://doi.org/10.4271/720506

Jung, W., & Oh, S. (1995). *The Influence of Vehicle Elements to Aspiration Wind Noise.* SAE Technical Paper 950624. doi:https://doi.org/10.4271/950624

Münder, M., & Carbon, C.-C. (2022). *Howl, whirr, and whistle: The perception of electric powertrain noise and its importance for perceived quality in electrified vehicles.* Applied Acoustics, Volume 185. doi:https://doi.org/10.1016/j.apacoust.2021.108412

Oettle, N., & Sims-Williams, D. (2017). *Automotive aeroacoustics: An overview.* Journal of Automobile Engineering, Volume 231, Issue 9. doi:https://doi.org/10.1177/0954407017695147

Qatu, M. S., Abdelhamid, M. K., Pang, J., & Sheng, G. (2009). *Overview of automotive noise and vibration.* International Journal of Vehicle Noise and Vibration, Vol. 5, No. 1-2. doi:https://doi.org/10.1504/IJVNV.2009.029187

Wang, Q., Chen, X., & Zhang, Y. (2021). *An Overview of Automotive Wind Noise and Buffeting Active Control.* SAE International Journal of Vehicle Dynamics, Stability, and NVH, 5(4). doi:https://doi.org/10.4271/10-05-04-0030

Yabu, T. (2026). *Derivation of Rossiter Formula in Cavity Resonance.* doi:https://doi.org/10.31224/7028

Zhang, F., Meng, W., Li, X., & Zheng, C. (2022). *A vehicle whistle database for evaluation of outdoor acoustic source localization and tracking using an intermediate-sized microphone array.* Applied Acoustics, Volume 201. doi:https://doi.org/10.1016/j.apacoust.2022.109113